



HAL
open science

Deletion of CTCF sites in the SHH locus alters enhancer-promoter interactions and leads to acheiropodia.

Aki Ushiki, Yichi Zhang, Chenling Xiong, Jingjing Zhao, Ilias Georgakopoulos-Soares, Lauren Kane, Kirsty Jamieson, Michael J Bamshad, Deborah A Nickerson, Yin Shen, et al.

► To cite this version:

Aki Ushiki, Yichi Zhang, Chenling Xiong, Jingjing Zhao, Ilias Georgakopoulos-Soares, et al.. Deletion of CTCF sites in the SHH locus alters enhancer-promoter interactions and leads to acheiropodia.. Nature Communications, 2021, Nature Communications, 12 (1), pp.2282. 10.1038/s41467-021-22470-z . hal-03344685

HAL Id: hal-03344685

<https://hal.univ-lille.fr/hal-03344685>

Submitted on 15 Sep 2021

HAL is a multi-disciplinary open access archive for the deposit and dissemination of scientific research documents, whether they are published or not. The documents may come from teaching and research institutions in France or abroad, or from public or private research centers.

L'archive ouverte pluridisciplinaire **HAL**, est destinée au dépôt et à la diffusion de documents scientifiques de niveau recherche, publiés ou non, émanant des établissements d'enseignement et de recherche français ou étrangers, des laboratoires publics ou privés.

1 **Peer review information:** *Nature Communications* thanks Marcelo Nobrega and the other, anonymous, reviewer(s) for their
2 contribution to the peer review of this work.

3
4 **Deletion of CTCF sites in the *SHH* locus alters enhancer-promoter interactions and leads to**
5 **acheiropodia**

6
7
8 Aki Ushiki^{1,2}, Yichi Zhang^{1,2,3}, Chenling Xiong^{1,2}, Jingjing Zhao^{1,2}, Ilias Georgakopoulos-Soares^{1,2},
9 Lauren Kane⁴, Kirsty Jamieson^{2,5}, Michael J. Bamshad^{6,7,8}, Deborah A. Nickerson^{7,8}, University of
10 Washington Center for Mendelian Genomics[#], Yin Shen^{2,5}, Laura A. Lettice⁴, Elizabeth Lemos
11 Silveira-Lucas⁹, Florence Petit¹⁰, Nadav Ahituv^{1,2}

12
13
14 ¹ Department of Bioengineering and Therapeutic Sciences, University of California San Francisco,
15 San Francisco, CA 94158, USA.

16 ² Institute for Human Genetics, University of California San Francisco, San Francisco, CA 94158,
17 USA.

18 ³ School of Pharmaceutical Sciences, Tsinghua University, Beijing, 100084, China

19 ⁴ MRC Human Genetics Unit, Institute of Genetics and Molecular Medicine, University of Edinburgh,
20 Crewe Road, Edinburgh EH4 2XU, UK

21 ⁵ Department of Neurology, University of California San Francisco, San Francisco, CA 94158, USA.

22 ⁶ Department of Pediatrics, University of Washington, Seattle, WA 98195, USA.

23 ⁷ Department of Genome Sciences, University of Washington, Seattle, WA 98195, USA.

24 ⁸ Brotman-Baty Institute, Seattle, WA 98195, USA.

25 ⁹ Consultorio Genetica Clinica, Porto Alegre, 90440, Brazil

26 ¹⁰ CHU Lille, University of Lille, EA7364 RADEME, F-59000, Lille, France.

27 [#] Please see the end of the file for the consortium author list. Non-contributing members of the
28 consortium are listed within the Supplementary Information file.

29
30 [Correspondence should be addressed to N.A. \(email:nadav.ahituv@ucsf.edu\).](mailto:nadav.ahituv@ucsf.edu)

33 **Abstract**

34 Acheiropodia, congenital limb truncation, is associated with homozygous deletions in
35 the *LMBR1* gene around ZRS, an enhancer regulating *SHH* during limb development. How these
36 deletions lead to this phenotype is unknown. Using whole-genome sequencing, we fine-mapped
37 the acheiropodia-associated region to 12 kb and show that it does not function as an enhancer.
38 CTCF and RAD21 ChIP-seq together with 4C-seq and DNA FISH identify three CTCF sites within
39 the acheiropodia-deleted region that mediate the interaction between the ZRS and
40 the *SHH* promoter. This interaction is substituted with other CTCF sites centromeric to the ZRS in
41 the disease state. Mouse knockouts of the orthologous 12 kb sequence have no apparent
42 abnormalities, showcasing the challenges in modelling CTCF alterations in animal models due to
43 inherent motif differences between species. Our results show that alterations in CTCF motifs can
44 lead to a Mendelian condition due to altered enhancer-promoter interactions.

45

46

47 **Introduction**

48 Acheiropodia (OMIM 200500) is a rare autosomal recessive disorder associated with bilateral
49 congenital transverse defects of the upper and lower limbs including aplasia of the hands and feet¹.
50 Genetic analysis of five Brazilian families with acheiropodia, three of which were consanguineous,
51 identified a homozygous deletion encompassing exon 4 of the limb development membrane protein
52 1 (*LMBR1*) gene to be associated with this phenotype². The deletion was estimated to cover 4-6
53 kilo base (kb) on either side of this exon. However, no assays were done to fine map the deletion
54 or functionally characterize how it could be causing acheiropodia.

55

56 While exon 4 of *LMBR1* was deleted in the individuals with acheiropodia, it is likely not the cause of
57 this phenotype. *LMBR1* is a membrane protein that is ubiquitously expressed³ and a 35 kb deletion
58 in mice that encompasses exons 1-3 of this gene did not lead to a limb phenotype⁴. *LMBR1*
59 contains an enhancer within intron 5, named the zone of polarizing activity regulatory
60 sequence (ZRS), that regulates the Sonic Hedgehog (*SHH*) gene during limb development. *SHH*
61 encodes a ligand that plays a major role in the development of several tissues, including the limb⁵.
62 In mice, *Shh* is expressed at the posterior part of the limb buds around embryonic day (E) 10-12^{6,7,8}
63 and plays a central role in digit patterning and limb outgrowth^{9,10}. *Shh* homozygous knockout mice
64 display early lethality with defective axial patterning and limb truncation reminding of acheiropodia¹⁰.
65 In humans, heterozygous pathogenic variants in *SHH* are responsible for a large spectrum of
66 central nervous system malformations without any limb malformation, of which the most severe is
67 holoprosencephaly (OMIM 142945)¹¹. Bi-allelic *SHH* disruption has not been described in humans.
68 Mutations in the ZRS, located ~1 Mb away of *SHH*, cause non-syndromic limb malformations in
69 humans, mice and many other species, consisting primarily of preaxial polydactyly due to ectopic
70 *SHH* expression in the limb bud^{12,13,14}. In addition, homozygous deletions encompassing the ZRS
71 lead to acheiropodia in humans and mice^{15,16}. Collectively, these results indicate that acheiropodia
72 is likely caused by reduced *SHH* expression during limb development. However, the ZRS is
73 completely intact in the Brazilian individuals with acheiropodia who are homozygous for the *LMBR1*
74 exon 4 deletion, suggesting that other functional units associated with *SHH* limb expression may be
75 disrupted by this deletion.

76

77 The architectural protein CCCTC-binding factor (CTCF) is known to play a central role in chromatin
78 conformation¹⁷. It is involved in forming topologically associating domain (TAD), regions in the

79 genome that are on average ~880 kb in length and are defined as having more frequent
80 interactions within this domain than outside it^{18,19}. In addition, CTCF is known to mediate long
81 range enhancer-promoter interactions¹⁷. CTCF-bound sites in a convergent orientation are thought
82 to halt chromatin loops that are progressively being extruded by the cohesin complex²⁰, facilitating
83 specific chromatin interaction. Previous studies in mice deleted individual and combinations of
84 CTCF sites in the *Shh* locus, some of them affecting interactions between the ZRS and *Shh*
85 promoter and leading to a reduction of up to ~52% of *Shh* expression in the limb, but none of which
86 led to an observable limb phenotype^{4,21}. Interestingly, ectopic CTCF sites appeared in these CTCF
87 motif knockout mice likely supporting compensatory interactions²¹.

88

89 We used whole-genome sequencing (WGS) to fine map the homozygous acheiropodia-associated
90 deletion in one of the probands from the Brazilian families, identifying a 12 kb deletion surrounding
91 *LMBR1* exon 4. Using a mouse transgenic enhancer assay, we show that this 12 kb sequence
92 does not have enhancer activity in the developing limb. Further analyses of this sequence using
93 CTCF and RAD21 ChIP-seq identified three CTCF sites in convergent orientation to *SHH* along
94 with RAD21 binding in this region. ChIP-seq analyses in the homozygous proband found an ectopic
95 CTCF site 27 kb centromeric to the ZRS. Consistent with these alterations of CTCF and RAD21
96 binding, interactions between the *SHH* promoter and the ZRS were found to be impaired in the
97 proband using 4C-seq and DNA fluorescence *in situ* hybridization (FISH). Finally, we generated a
98 mouse knockout of the orthologous 12 kb acheiropodia-associated region and did not find any limb
99 malformations, highlighting the differential chromatin interactions in this locus in mice compared to
100 humans. Combined, our results suggest that, in humans, CTCF sites adjacent to the ZRS are likely
101 needed as a scaffold to associate the *SHH* promoter to the ZRS and that this mechanism is
102 different in mice.

103

104 Results

106 Whole-genome sequencing identifies a 12 kb acheiropodia-associated deletion

107 We obtained genomic DNA and lymphoblastoid cell lines from a female proband with acheiropodia
108 and her parents. The proband has terminal transverse hemimelia of the four limbs with truncation
109 of both hands and feet²². Prior genetic testing identified a deletion overlapping exon 4 of the
110 *LMBR1* gene with an estimate for the deletion's boundaries to be around 1.2–2.5 kb and 2.7–3.5 kb
111 5' and 3' of exon 4 respectively². To identify the exact deletion coordinates and assess whether
112 other pathogenic variants might explain the phenotype, we carried out WGS on the proband and
113 her parents. Because of known consanguinity (**Fig. 1a**), we searched for regions of homozygosity
114 in the proband, finding runs spanning a total of 302 mega base (Mb) within the genome
115 (**Supplementary Table 1**). Previous genomic analyses of five consanguineous families with
116 acheiropodia, including this family (Family 2 in²), found that all of them share a ~0.5 Mb region of
117 homozygosity in the *LMBR1* gene locus. Based on these results and the known deletion of exon 4,
118 we focused our analyses on this region, identifying a 4 Mb region of homozygosity from
119 rs12719966 to rs1985369 (chr7:155,356,342- 159,326,530; hg38). No pathogenic or likely
120 pathogenic variants were found in *SHH*. In the proband, we identified a 12,041 base pair (bp)
121 homozygous deletion (chr7:156,816,030-156,828,070; hg38) that overlaps *LMBR1* exon 4 along
122 with two base pairs (CA) that were inserted at the breakpoint (**Fig. 1b-d**, **Supplementary Fig. 1**).
123 Both unaffected parents are heterozygous for this deletion (**Fig. 1b-c**, **Supplementary Fig. 1**). We
124 reported this deletion in the Decipher database²³ (#411659) and did not identify any overlapping
125 homozygous deletions in control databases²⁴. To further validate our WGS results, we carried out
126 both PCR analyses around the breakpoint (**Fig. 1c**) and Sanger sequencing of the breakpoint (**Fig.**
127 **1d**, **Supplementary Fig. 1**), the results of which corroborated our findings.

129 As homozygous deletions of the ZRS, which regulates *SHH* expression in the developing limb,
130 were shown to lead to truncated limbs in mice and humans^{15,16}, we carried out detailed sequence
131 analysis of this enhancer. WGS and Sanger sequencing analyses of the ZRS (chr7:156,790,916-
132 156,792,095; hg38) in the proband affected with acheiropodia did not reveal any rare variants in
133 this enhancer. We did observe a homozygous single nucleotide polymorphism (SNP) rs10254391
134 (chr7:156,791,873; hg38) in the proband and that was heterozygous in both parents. As this SNP
135 has a minor allele frequency of 0.26 in the global population, has been reported to be homozygous

136 in around 1,702 cases in GnomAD²⁵ and is thought to be benign based on the ClinVar database²⁶,
137 we concluded that it is not likely to be causative of this phenotype. Our results strongly suggest that
138 the acheiropodia in the proband is likely caused by the 12 kb homozygous deletion.

140 **The 12 kb deleted region does not function as a limb developmental enhancer**

141 To test whether this region functions as a developmental limb enhancer, we tested its ability to
142 drive limb expression in mouse embryos. We amplified this 12 kb sequence from a human BAC
143 (RP11-155D20), cloned it into the *Hsp68*-LacZ vector, that contains an *Hsp68* minimal promoter
144 followed by the LacZ reporter gene²⁷, and injected it into one-cell mouse embryos (**Fig. 2**).

145 Transgenic embryos were harvested at E11.5, a time point that is critical for *Shh* limb expression in
146 the zone of polarizing activity (ZPA^{6,16}). We obtained six LacZ PCR positive embryos, three not
147 showing any LacZ expression whatsoever and three having inconsistent LacZ expression, none of
148 which have expression in the ZPA (**Fig. 2**). Previous studies have tested ZRS human
149 sequences/mutations in mice using this assay, finding LacZ expression in the ZPA^{28,29}. We also
150 checked this 12 kb region for the presence of various histone modifications indicative of enhancer
151 activity from ENCODE³⁰ genomic data. Analysis of 18 different cell types found only a poised
152 enhancer mark, H3K4me1, in two of the cell lines, K562 and A549 (**Supplementary Fig. 2**).
153 Combined, these results strongly suggest that this 12 kb region does not function as an enhancer
154 in general and more specifically in the ZPA at E11.5.

156 **The 12 kb deletion leads to altered CTCF/RAD21 distribution**

157 We next analyzed the 12 kb deleted region for potential functional entities that could lead to the
158 acheiropodia phenotype. While it overlaps exon 4 of the *LMBR1* gene, mouse knockouts of this
159 gene do not have any apparent limb phenotype⁴, the numerous mutations that were identified in it
160 in humans and mice are thought to lead to limb malformations due to altering ZRS copy number or
161 sequence¹² and an acheiropodia phenotype was observed in both *Shh* and ZRS homozygous
162 mouse knockouts^{10,16} and homozygous ZRS deletion in humans¹⁵. We reasoned that the likely
163 cause of the acheiropodia in this proband is altered *SHH* expression during limb development.
164 Analysis of ENCODE³⁰ ChIP-seq datasets identified three CTCF-bound sites in this region, named
165 here as *LMBR1-SHH* CTCF (LSC) sites 3-5. These three CTCF-bound sites appear in numerous
166 ChIP-seq assays (LSC3: 118/191, LSC4: 97/191, LSC5: 139/191) from various human cell lines,
167 strongly suggesting that they are functional (**Supplementary Fig. 3, Supplementary Table 2**). As

168 CTCF motif orientation was shown to be important in determining the positioning of chromatin
169 looping³¹, we next analyzed the orientation of these sites. We found that all three sites are in
170 convergent orientation to the *SHH* gene (**Fig. 3a**). We thus speculated that this 12 kb region may
171 function as a scaffolding region, enabling ZRS to interact with the *SHH* promoter.

172
173 To test whether this sequence functions as a scaffolding region, we carried out ChIP-seq for both
174 CTCF and RAD21, a member of the cohesin complex that along with CTCF is known to determine
175 chromatin looping³². ChIP-seq was done for both proteins using proband and wild type
176 lymphoblastoid cells. It is important to note that these cells were established using an Epstein Barr
177 virus which could affect our subsequent genomic studies. As a previous study²¹ indicated that the
178 interaction between *Shh* and ZRS is “tissue-invariant”, we reasoned that these cells could be used
179 for these analyses. We also checked the mRNA expression of *SHH* in the wild type and mutant
180 cells, observing overall low expression levels that were significantly higher in wild-type versus
181 proband cells (**Supplementary Fig.4**). In the wild type cells, we observed three CTCF ChIP-seq
182 peaks (LSC3-5) that have sites in convergent orientation to *SHH* and correspond to those found in
183 the ENCODE datasets (**Fig. 3a-b, Supplementary Fig. 5-6**). For RAD21, we also observed
184 binding in the 12 kb region, in particular at the LSC3 site (**Fig. 3a-b, Supplementary Fig. 5-6**). In
185 the proband’s cells, we did not observe the CTCF and RAD21 peaks due to the 12 kb deletion.
186 Instead, we observed a novel RAD21 and CTCF peak in convergent orientation to *SHH* (LSC2)
187 near exon 6 of *LMBR1* that does not appear in wild type cells (**Fig. 3a-b, Supplementary Fig. 5-6**).

188
189 We next analyzed the CTCF motif scores of LSC1-5 to assess whether they could be associated
190 with the appearance of the novel CTCF binding (LSC2) observed in the proband’s cell line. We
191 used the Find Individual Motif Occurrences (FIMO³³) tool to assign motif scores for all five sites. We
192 extracted the CTCF motifs with a p-value threshold of 0.001 genome-wide and only picked motifs in
193 the *SHH-LMBR1* locus that overlapped CTCF peaks in our ChIP-seq. For LSC3-5, we observed
194 motif scores, determined by the weights at the corresponding position weight matrix summing up to
195 16, 5.2 and 17 respectively, while for LSC2 we obtained a score of 11 (**Fig. 3c**). This suggests that
196 with the loss of LSC3-5 due to the deletion, CTCF might bind to the LSC2 weaker binding affinity
197 motif instead of LSC3-5.

198
199 **The 12 kb deletion impairs the interaction between ZRS and the *SHH* promoter**

200 To examine whether the chromatin interaction between the ZRS and the *SHH* promoter are altered
201 due to the 12 kb deletion, we performed 4C-seq using the *SHH* promoter as a viewpoint. 4C-seq
202 was performed on both proband and wild type lymphoblastoid cell lines using standard methods³⁴
203 (see Methods). In wild type cells, we observed that the *SHH* promoter strongly interacts with LSC1
204 and LSC3-5 (**Fig. 4a, Supplementary Fig. 5-6**). For the proband's cells, we did not observe
205 interactions with the ZRS and instead saw increased interactions between the *SHH* promoter and
206 LSC1 (**Fig. 4b, Supplementary Fig. 5-6**). Interestingly, in wild type cells we observed a weak
207 interaction with the ZRS compared to a much stronger interaction between LSC3-5 and the *SHH*
208 promoter (**Fig. 4b, Supplementary Fig. 5-6**). We also analyzed published CTCF Hi-ChIP data
209 from human GM12878 lymphoblastoid cells³⁵ and observed a much more robust interaction
210 between the *SHH* promoter and the 12 kb region compared to the ZRS (**Supplementary Fig.7**).
211

212 DNA FISH was also carried out on both proband and parental lymphoblastoid cell lines to
213 investigate chromosome conformation changes in an allele-specific manner using probes targeting
214 the *SHH* promoter, LSC1, LSC2 and LSC3-5 (**Fig. 5a**). To distinguish between the wild type and
215 mutant alleles in the parental cell lines, we used a plasmid containing the 12 kb acheiropodia-
216 associated region (**Fig. 5b**). LSC1 was found to be significantly closer to the *SHH* promoter on the
217 mutant allele compared to the wild type chromosome, suggestive of an increased interaction
218 between LSC1 and the *SHH* gene. We also observed that the novel LSC2 peak identified in the
219 proband's cell line is not found closer to the *SHH* promoter when comparing the wild type allele to
220 the mutant (**Fig. 5c**). However, we did observe a significant increase in the distance between the
221 *SHH* promoter and the region containing the 12 kb deletion that was specific to the mutant allele
222 consistent with the loss of interactions observed by 4C-seq (**Fig. 4**). These results further suggest
223 that the 12 kb acheiropodia-associated region functions as a scaffolding region between the ZRS
224 and the *SHH* promoter and its deletion impairs this interaction.
225

226 **Removal of the acheiropodia-associated region in mice does not lead to an observable** 227 **phenotype**

228 To further assess the function of this sequence in mice, we generated a mouse knockout of the
229 orthologous 12 kb acheiropodia-associated region. Using the liftOver tool in the UCSC Genome
230 Browser³⁶ (see methods) the human 12 kb acheiropodia-associated sequence was converted to its
231 orthologous mouse sequence (chr5:29,335,354-29,348,393; mm10). Of note, using FIMO³³ we

232 observed that mice have eight CTCF motifs in this orthologous region while humans have four, and
233 only one of the eight overlapped mouse limb CTCF ChIP-seq data^{37,38} (**Fig. 6a**). We also analyzed
234 developing mouse embryonic limb (E10.5-E15.5) ChIP-seq datasets for various histone
235 modifications (H3Kme1, H3K4me2, H3K4me3, H3K9ac, H3K9me3, H3K27ac, H3K27me3,
236 H3K36me3) and ATAC-seq from ENCODE³⁰ and did not observe any peaks overlapping this
237 region (**Supplementary Fig. 8**). Previous deletions of various CTCF sites in this region in mice did
238 not show any apparent limb malformations^{4,21}. However, these deletions did not cover the
239 acheiropodia-associated region (**Fig. 6a**). We generated a knockout mouse which harbors the
240 orthologous 12 kb acheiropodia-associated deletion along with additional sequence due to sgRNA
241 selection constraints (chr5:29,334,962-29,348,393; mm10). Mouse knockouts were generated
242 using the improved-Genome editing via Oviductal Nucleic Acids Delivery (*i*-GONAD³⁹) technique.
243 Founder mice and germ line transmission in F1 offspring with the desired deletion were validated
244 by PCR, Sanger sequencing and Southern blot (**Supplementary Fig. 9**). We focused our
245 subsequent phenotypic analyses on mouse line 517 that had a single nucleotide T insertion within
246 the deleted region (**Supplementary Fig. 9a**).

247
248 To determine the functional effect of the deletion, we generated homozygous mice and phenotyped
249 them using qRT-PCR, whole mount *in situ* hybridization (WISH) and alizarin red/alcian blue skeletal
250 staining. Homozygous mice did not have any observable phenotype. qRT-PCR on E11.5 autopods
251 from both forelimbs and hindlimb did not identify *Shh* expression changes between homozygous
252 and wild type mice (**Fig. 6b**). WISH for *Shh* did not identify any changes in expression between
253 homozygous and wild type E11.5 embryos (**Fig. 6c**). Finally, we checked the limb skeletal structure
254 at E18.5 using alizarin red/alcian blue staining finding no apparent abnormalities in the
255 homozygous embryos (**Fig. 6d**). These results highlight that mice are not an appropriate model to
256 test the chromosomal interactions in humans for this region, likely due to the differences in CTCF
257 site distribution and orientation. In addition, they also suggest that removal of *Lmbr1* exon 4 does
258 not lead to a limb-associated phenotype in mice.

260 Discussion

261
262 We identified a 12 kb homozygous deletion that is associated with acheiropodia. We show that this
263 12 kb region does not have enhancer activity at mouse E11.5. Our CTCF and RAD21 ChIP-seq
264 data indicate that this region has three CTCF binding sites along with RAD21 binding (**Fig. 3b**).
265 Chromatin interaction analyses of this region suggests that it functions as a scaffolding region
266 between the ZRS and the *SHH* promoter via three CTCF sites (LSC3-5). In the cells from the
267 proband with acheiropodia, these sites are deleted and this interaction is substituted with another
268 CTCF site (LSC1) centromeric to the ZRS. Due to this change in interaction, the ZRS does not
269 interact with the *SHH* promoter (**Fig. 7**). Deletion of the orthologous region in mice did not lead to
270 an observable phenotype, likely due to the inherent chromatin interaction and CTCF distribution
271 differences between humans and mice in this region.

272
273 Our work suggests there are substantial differences in the regulation of chromosomal interactions
274 linking ZRS to the *SHH* promoter between humans and mice. There are two previous reports that
275 generated CTCF site-specific deletions around the ZRS in mouse^{4,21}. Paliou *et al.*²¹ deleted the i4[#]
276 or i5[#] CTCF sites (**Fig. 6a**) individually or together and observed no major limb phenotype even
277 though a 51% reduction of *Shh* expression was observed in E10.5 limb buds when both CTCF
278 sites were deleted. Following the deletion of these two CTCF sites (i4[#] and i5[#]), ectopic CTCF sites
279 also appeared, one within the ZRS (ZRS[#]) and the other near the transcription start site (TSS) of
280 *Lmbr1* (termed here as i3[#]), both of which do not overlap our observed ectopic CTCF site, LSC2
281 (**Fig. 6a**). To characterize the function of the ectopic CTCF sites, three sites (i4[#], i5[#] and ZRS[#])
282 were deleted, leading to a depletion of all CTCF (including i3[#]) and RAD21 binding around the ZRS
283 and significantly decreasing the interaction between *Shh* and ZRS. Although these triple deletions
284 led to a 52% reduction of *Shh* expression in E10.5 limb buds, no limb abnormalities were observed.
285 Williamson *et al.*⁴ deleted three different CTCF sites individually around the *Shh* gene and ZRS
286 (CTCF3*, 4*, and 5*; **Fig. 6a**). Mice homozygous for each deletion did not show an observable limb
287 phenotype. They also generated a homozygous 35 kb deletion that contains CTCF4*, i3[#], 5* and
288 the *Lmbr1* TSS and promoter and did not observe *Shh* gene expression changes in E11.5 limb
289 buds measured by qRT-PCR and any apparent limb abnormalities. Of note, as previously
290 mentioned, these results also suggest that *Lmbr1* itself is not necessary for limb development, as
291 also observed in our 12 kb knockout mice. Combined, these CTCF mouse deletion studies,

292 including our study, imply that ZRS-*Shh* interactions are likely to be robust to individual or even
293 triple CTCF perturbations. They also suggest that other CTCF sites, either those that were not
294 tested in these studies or ones that appear ectopically following these manipulations, keep this
295 interaction intact.

296
297 The phenotypic differences between human and mice are likely due to several factors including
298 differences in CTCF location, motif score and orientation. In terms of location, humans have three
299 CTCF ChIP-seq peaks (LSC3-5) in the deleted region; however, mouse has one CTCF peak in the
300 orthologous 12 kb acheiropodia deleted sequence (*i4*[#]) and this region does not show strong
301 evolutionary conservation between humans and mice (**Fig. 6a**). Our work suggests that these three
302 human CTCF sites (LSC3-5) play a role as an anchor/scaffolding region for the interaction between
303 ZRS and the *SHH* promoter. In mice, *i4*[#] and *i5*[#] likely play this role and their relative distal position
304 between one another might be important for robustness. Analysis of previously published 4C-seq
305 from E10.5 mouse limbs²¹ showed interactions between the *Shh* promoter and *i9*[#], CTCF3*/*i5*[#] and
306 ZRS[#] but not with the 12 kb acheiropodia-associated region (**Supplementary Fig. 10**). These
307 CTCF sites could be working cooperatively to maintain the interaction between ZRS and the *Shh*
308 promoter. For LSC1, where we observed increased interactions with the *SHH* promoter in the
309 proband, CTCF ChIP-seq from ENCODE³⁰ has 161/191 assays showing CTCF-bound sites in this
310 region while in ChIP-seq datasets from various mouse tissues/cells we only observed about half of
311 the assays to have a peak in this region (**Supplementary Fig. 11**). Interestingly, for LSC2, while
312 we only observed a CTCF ChIP-seq peak in the proband, likely due to compensation for the
313 deletion of LSC3-5, in mice the homologous CTCF site, 3*/*i5*[#], shows a strong CTCF ChIP-seq
314 peak in wild-type E10.5, E13.5 and E14.5 limbs (**Fig. 6a**) and in ENCODE³⁰ mouse datasets
315 (**Supplementary Fig. 11**). Analyses of CTCF motif scores for LSC2 versus 3*/*i5*[#] shows a weaker
316 score for LSC2 (**Supplementary Fig. 12a**), and this CTCF site also has a weak interaction with the
317 *SHH* promoter (**Fig. 4**). Weaker CTCF sites might serve as a backup for failed enhancer-promoter
318 interactions. Correspondingly, analyses of ZRS[#] and *i3*[#] ectopic CTCF sites which appeared in the
319 *i4*[#] and *i5*[#] double deletion mice found them to have lower motif scores than *i4*[#] and *i5*[#]
320 (**Supplementary Fig. 12b**).

321
322 In terms of orientation, all three CTCF sites in the 12 kb acheiropodia-deleted region (LSC3-5) are
323 in convergent orientation to *SHH* along with LSC1 and LSC2, while the sites telomeric to LSC5,

324 LSC6 and LSC7, are in divergent orientation or both (**Fig 6a**). In mice, CTCF site 4* that is
325 homologous to LSC6 and 5* which is homologous to LSC7 are all in divergent orientation to *Shh*,
326 but i3[#] is in convergent orientation (**Fig 6a**). Carrying out a more global analysis of human and
327 mouse CTCF ChIP-seq peaks that compared human K562 to mouse CH12 cells, both
328 lymphoblasts, shows that only around 25% of the peaks overlap when converting their coordinates
329 to mouse or vice versa (**Supplementary Fig. 13**). These results are consistent with a recent report
330 that also analyzed the overlap of CTCF ChIP-seq peaks between these cells (K562 and CH12)
331 plus human GM12878 and mouse MEL cells⁴⁰. This suggests that there are major differences
332 between human and mouse in terms of CTCF location. These differences could be due to various
333 selection pressures, proving more safeguards for enhancer-promoter interactions. It will also be
334 intriguing to test whether these changes in CTCF location and orientation could be involved in
335 phenotypic differences between species. Taken together, our results highlight that mouse is not a
336 useful model to assess the chromatin interactions in humans for this locus and that CTCF location,
337 orientation and number needs to be assessed between human and mice before using mice as an
338 animal model to dissect human nucleotide variation that affects CTCF binding.

339

340 The 12 kb acheiropodia-associated deleted region resides close to a topologically associated
341 domain (TAD) boundary that encompasses both *SHH* and *LMBR1*. Previous mouse genetic studies
342 have shown that TAD boundary alterations could alter chromatin interactions and lead to ectopic
343 gene expression^{31,41}. While we cannot definitively exclude that this deletion is associated with TAD
344 boundary alterations, using the 3D Genome Browser⁴², we have analyzed this TAD boundary in Hi-
345 C datasets from ten different human cell lines, finding that in all of them the boundary does not
346 overlap this 12 kb deleted region. We observed two different locations for this boundary that differ
347 between cell types. For five of the cell lines (HepG2, GM12878, NHEK, K562 and HMEC), this
348 boundary is thought to be located around the *LMBR1* TSS while for five other cell lines (H1-ESC,
349 G401, A549, epidermal keratinocyte and hippocampus) the boundary is estimated to be around the
350 transcription termination site of the DnaJ heat shock protein family (Hsp40) member B6 (*DNAJB6*)
351 gene (**Supplementary Fig. 14**). Human and mice TAD boundaries were shown to be relatively
352 conserved⁴³. In mice, the *Shh-Lmbr1* TAD boundary resides around the *Lmbr1* TSS⁴⁴, similar to
353 what is observed in humans for five out of the ten cell lines. Symmons *et al.*⁴⁴ inverted a 450 kb
354 region (300 kb downstream and 150 kb upstream of *Lmbr1*) that contains this boundary. This led to
355 a complete loss of *Shh* expression in the ZPA and a limb truncation phenotype, similar to the ZRS

356 homozygous knockout. 4C-seq analysis revealed that the ZRS-*Shh* interaction was disrupted in
357 this inversion, further suggesting that altering this interaction can lead to an acheiropodia like
358 phenotype. In summary, while we cannot conclusively rule out that alteration of the TAD boundary
359 is responsible for this phenotype, our results strongly suggested that removal of these CTCF sites
360 in humans alters the interaction between ZRS and the *SHH* promoter, likely leading to the
361 acheiropodia phenotype.

362
363 CTCF plays a major role in enhancer-promoter interactions, facilitating transcriptional activity by
364 establishing chromatin loops between these elements^{45,46}. However, only a small number of
365 genetic diseases where CTCF site-specific mutations lead to alterations of these enhancer-
366 promoter interactions have been reported. CTCF site-specific deletions were shown to be
367 associated with imprinting in the *IGF2/H19* locus, causing Beckwith-Wiedemann syndrome (BWS;
368 OMIM 130650). A 1.8 kb deletion that removes two CTCF sites in the normal imprinted and
369 silenced *IGF2* expression in the maternal allele was shown to lead to hypermethylation and biallelic
370 expression of *IGF2* and is thought to cause BWS⁴⁷. Several reports have associated somatic
371 mutations in CTCF sites with various cancers^{48,49}. Interestingly, analysis of somatic mutations from
372 the International Cancer Genome Consortium database⁵⁰ revealed that numerous mutations
373 overlap human stem cell CTCF loop anchors⁵¹, suggesting that aberrant chromatin interactions
374 could be strongly associated with cancer. To our knowledge, this study is the first report a CTCF
375 mutation that is associated with a Mendelian condition. With WGS becoming more commonly used
376 in the clinic, it would be interesting to analyze disease-associated variants, in particular short indels,
377 for their overlap with CTCF motifs and chromatin interactions. In addition, our study shows that due
378 to differences in CTCF site location, motif sequence and orientation animal models may not be a
379 good proxy to analyze the effects of CTCF site variation. As more human genomes are sequenced
380 and the genomes of additional species become available, it will be important to consider the
381 phenotypic effects of nucleotide changes in CTCF sequences on disease and evolution.

383 **Methods**

385 **Patient sample collection**

386 The study was approved by the ethical committee of the University of California San Francisco,
387 protocol number 10-03111, Comitê de Ética em Pesquisa da Prefeitura de Porto Alegre
388 (Plataforma Brasil) protocol number 1.103.654 and the Brazilian Research Ethics Commission
389 (CONEP) protocol number 223.811. Samples were obtained after receipt of informed consent.
390 Genomic DNA was extracted from saliva using standard techniques. Blood samples were collected
391 using standard techniques and used for the generation of lymphoblastoid cell lines. Clinical data
392 were obtained from a physician examination and review of medical records.

394 **Establishment of lymphoblastoid cell line and culture**

395 Blood samples from the proband and parents were spun over Ficoll-Paque (Amersham
396 Biosciences) gradients to enrich the sample for mononuclear cells. Epstein Bar virus (EBV)-
397 transformed lymphoblastoid lines were generated from isolated peripheral blood
398 lymphocytes. Briefly, cells were washed and resuspended in complete Iscove's modified
399 Dulbecco's culture media supplemented with 10% v/v fetal bovine serum, antibiotics, and virus.
400 The B95-8 EBV-infected marmoset cell line (ATCC, catalog no. CRL-1612) was used as the source
401 for viral stocks. High molecular weight DNA was isolated from Ficoll-Paque enriched mononuclear
402 cells using standard desalting procedures. Lymphoblastoid cells were maintained in RPMI1640
403 medium (Life Technologies, catalog no. 11875093) containing 15% fetal bovine serum (FBS) and
404 penicillin-streptomycin.

406 **Whole genome sequencing**

407 Whole genome sequencing was performed at the University of Washington Center for Mendelian
408 Genomics (University of Washington, Seattle). Initial quality control (QC) entailed DNA
409 quantification, gender validation assay and molecular fingerprinting with a 63-SNP OpenArray
410 assay derived from a custom exome SNP set. Following successful QC, at least 750 ng of genomic
411 DNA was subjected to a series library construction steps utilizing the KAPA Hyper Prep kit (Roche),
412 automated on the Perkin Elmer Janus platform. Libraries were validated using the Bio-Rad CFX384
413 Real-Time System and KAPA Library Quantification kit (Roche). Samples were sequenced on a
414 HiSeq X using Illumina's HiSeq X Ten Reagent Kit (v2.5) to an average depth of 30X. Burrows-
415 Wheeler Aligner⁵², Genome Analysis ToolKit⁵³ and SeattleSeq Annotation server build 138

416 (<https://snp.gs.washington.edu/SeattleSeqAnnotation138/>) were used to generate BAM, vcf and
417 annotation files, respectively. Homozygosity mapping was performed with PLINK v1.07 software⁵⁴
418 using the genotypes generated by the 63-SNP OpenArray assay. Structural variants were called
419 using Lumpy⁵⁵. Alignments were visualized using the Integrative Genomics Viewer tool⁵⁶. The
420 *LMBR1* deletion and ZRS variants were validated by PCR-Sanger sequencing (primers provided in
421 **Supplementary Table 3**).

423 **Mouse transgenic enhancer assays**

424 Mouse work was approved by the UCSF Institutional Animal Care and Use Committee (IACUC),
425 protocol number AN100466, and was conducted in accordance with AALAC and NIH guidelines.
426 The 12 kb acheiropodia associated region was amplified from a human BAC (RP11-155D20) by
427 PCR, cloned it into the *Hsp68-LacZ* vector²⁷ and sequence verified. All LacZ transgenic mice were
428 generated by Cyagen Biosciences using standard procedures⁵⁷, and harvested and stained for
429 LacZ expression at E11.5 as previously described⁵⁸. Pictures were obtained using an M165FC
430 stereo microscope and a DFC500 12-megapixel camera (Leica).

432 **ChIP-seq**

433 Lymphoblastoid cells were plated on two different flasks and used for the experiment as
434 independent tubes considered as two technical replicates. Cells (1×10^7 cells) were fixed in
435 phosphate-buffered saline (PBS) with 0.96% formaldehyde for 8 minutes at room temperature.
436 Crosslinking was quenched with 125 mM Glycine. The cells were washed with PBS and
437 precipitated via centrifugation. The cell pellet was stored in -80°C until use. The pellet was lysed in
438 240 μL of Buffer B (LowCell# ChIP kit; Diagenode, catalog no. C01010072) and lysed chromatin
439 was sheared using a Covaris S2 sonicator to obtain on average 250 bp size fragments. **ChIP was**
440 **performed using the LowCell# ChIP kit according to manufacturer's protocol with modifications. 120**
441 **μL of sheared chromatin was mixed with 880 μL of Buffer A (LowCell# ChIP kit) supplemented with**
442 **complete protease inhibitor (Sigma-Aldrich, catalog no. 11873580001). 80 μL of the solution was**
443 **saved as input control. To obtain magnetic bead-antibody complexes, 22 μL of protein A-coated**
444 **paramagnetic beads (LowCell# ChIP kit) were washed twice with Buffer A (LowCell# ChIP kit) and**
445 **resuspended in 22 μL of Buffer A. 10 μL of magnetic beads were mixed with 90 μL of Buffer A**
446 **(LowCell# ChIP kit) and 6 μg antibody (final antibody concentration was 60 ng/ μL in the binding**
447 **reaction). This mixture was gently agitated at 4°C for 2 hours. Antibody against CTCF (Active Motif,**

448 catalog no. 61311) or RAD21 (Abcam, catalog no. ab992) was used for immunoprecipitation
449 respectively. The bead-antibody complex was precipitated with a magnet and the supernatant was
450 removed. 800 mL of shared chromatin was added to the bead-antibody complex and rotated at 4°C
451 overnight. The beads were then washed with Buffer A three times and Buffer C once. DNA was
452 purified using IPure kit v2 (Diagenode, catalog no. C03010015) according to the manufacturer's
453 protocol. Sequencing libraries were generated using the Accel-NGS 2S Plus DNA Library Kit (Swift
454 Biosciences, catalog no. 21024) according to manufacturer's protocol. Massively parallel
455 sequencing was performed on an Illumina HiSeq4000 with 50 bp single-end read. ChIP-seq was
456 done with two technical replicates. ChIP-seq data was analyzed following the ENCODE
457 transcription factor pipeline⁵⁹. Both RAD21 and CTCF ChIP-seq raw reads were mapped against
458 the human genome (GRCh37; hg19) using bowtie2 (v2.2.6). Duplicate reads were marked using
459 Picard (v1.126) MarkDuplicates and multimapping, low quality, duplicated and non-properly paired
460 reads were removed. Library complexity measures and flagstats were generated for each BAM file.
461 BAM files were converted to tagAlign format and two subsampled pseudoreplicates were
462 generated for each sample with half the total reads. Reproducible peaks were identified using the
463 MASC2 (v2.1.1)⁶⁰ peak caller and the irreproducibility discovery rate (IDR (v2.0.4)) framework⁵⁹.
464 IDR analysis was performed using self-pseudoreplicates and the main samples to obtain self-
465 consistent sets of peaks. Final peak calls were filtered using the ENCODE blacklist⁶¹ and an IDR of
466 2% with a signal value > 30. We combined replicates to obtain only highly reproducible peaks using
467 the IDR⁵⁹ and show them pooled in main figure and individual replicates in supplementary figures.
468 Differential enrichment analysis between the proband and wild type cells was performed by
469 DiffBind⁶².

471 **CTCF motif analysis**

472 We used the position-weight matrix MA0139.1 from JASPAR⁶³ to scan for CTCF motifs. Genome-
473 wide CTCF motif identification was performed on the human (hg19) and mouse (mm9) genomes,
474 with FIMO³³, with a p-value threshold of 0.0001. For some CTCF peaks in the *SHH-LMBR1* locus
475 (LSC4, 6, and 7), when there was no CTCF motif that overlapped ChIP-seq peaks, we reduced the
476 p-value threshold to 0.001. CTCF orientation was determined by the strand in which the motif was
477 identified. For the human-mouse CTCF ChIP-seq comparisons, experiments from the cell lines
478 K562³⁰ and CH12³⁷ were analyzed. The UCSC Genome Browser³⁶ liftOver tool was used with –

479 minMatch=0.01 to transfer the peak coordinates between the two species followed by BEDtools⁶⁴
480 to intersect them and calculate the proportion of overlapping peaks.

482 **4C-seq**

483 Lymphoblastoid cells were plated on two different flasks and used for the experiment as
484 independent tubes deemed as two technical replicates. 4C-seq was performed using standard
485 procedures³⁴. Briefly, 1×10^7 cells were fixed in PBS with 2% formaldehyde for 10 minutes at room
486 temperature. Crosslinking was quenched with 125 mM Glycine. The cells were precipitated via
487 centrifugation and resuspended in lysis buffer (50 mM Tris-HCl pH7.5, 150 mM NaCl, 5 mM EDTA,
488 0.5% NP-40, 1.15% Triton X-100, 1x complete proteinase inhibitors (Roche, catalog no.
489 11697498001)) and incubated for 10 minutes on ice. They were then precipitated via centrifugation
490 and washed with PBS. The cell pellet was stored in -80°C until use. The cell pellet was suspended
491 in *DpnII* restriction enzyme buffer and treated with 0.3% SDS and 2.5% Triton X100 at 37°C for 1
492 hour, respectively. Chromatin was digested with 100 units of *DpnII* (New England Biolabs, catalog
493 no. R0543) at 37°C for 3 hours. An additional 100 unit of *DpnII* was added and the reaction was
494 incubated at 37°C overnight. After heat inactivation of the enzyme, 50 units of T4 DNA ligase
495 (Roche, catalog no. 10799009001) were applied for self-ligation of the digested chromatin and
496 placed for incubation at 16°C overnight. After purification of DNA using phenol-chloroform and
497 ethanol precipitation, DNA was digested with 50 units of *NlaIII* (New England Biolabs, catalog no.
498 R0125) at 37°C overnight. Following heat inactivation of the enzyme at 65°C , 25 μg of DNA was
499 used for the second ligation reaction with 50 units of T4 DNA ligase at 16°C overnight. After
500 purification of DNA using phenol-chloroform and ethanol precipitation, the inverse PCR was
501 performed using NEBNext high-fidelity 2X PCR master mix (New England Biolabs, catalog no.
502 M0541). DNA was purified with AMPure XP beads (Beckman Coulter, catalog no. A63881). The
503 second round of PCR was performed using NEBNext high-fidelity 2X PCR master mix to attach
504 library adapters and index sequences. All PCR primer sequences are listed in **Supplementary**
505 **Table 3**. DNA was purified with the QIAquick PCR purification kit (Qiagen, catalog no. 28104).
506 Massively parallel sequencing was performed on an Illumina HiSeq4000 with 50 bp single-end
507 reads using a custom primer (**Supplementary Table 3**). 4C-seq was carried out using two
508 technical replicates. 4C-seq data was analyzed using the 4C-seq pipeline⁶⁵. [Briefly, 4C-seq raw](#)
509 [reads were trimmed to 50 bp with cutadapt 2.4. Valid 4C-seq reads containing 4C reading primer](#)
510 [were extracted from fastq file and parsed into raw.txt file aligned against the restriction-enzyme](#)

511 digested genome GRCh37(hg19) using 4Cseqpipe version 0.7⁶⁵. Raw files were translated into
512 final graphical depictions of contact profiles around viewpoints using 4Cseqpipe version 0.7⁶⁵.

514 DNA FISH

515 For DNA FISH, $0.5-1 \times 10^6$ lymphoblastoid cells were seeded on Poly-prep slides (Sigma) overnight.
516 They were then fixed in 4% paraformaldehyde for 10 minutes at room temperature and
517 permeabilized using 0.5% Triton X for 10 minutes⁶⁶. Fosmid clones and plasmid were prepared
518 and labelled as previously described⁶⁷. Cells were denatured for 30 minutes. For four-color FISH,
519 each slide was hybridized with between 80-100 ng of biotin-, digoxigenin- and directly labelled
520 probes, 18 μ g of human Cot1 DNA (Invitrogen) and 5 μ g salmon sperm DNA. Green496-dUTP
521 (Enzo Life Sciences) was used for direct labelling of fosmid probes. Washes and detection were as
522 previously described⁶⁷. See **Supplementary Table 3** for Fosmid probe details.

523
524 Slides were imaged using a Photometrics Coolsnap HQ2CCD camera and a Zeiss AxioImager A1
525 fluorescence microscope with a Plan Aplanachromat 100 \times 1.4NA objective, a Nikon Intensilight
526 Mercury based light source and either Chroma #89014ET (three-colour) or #89000ET (four-colour)
527 single excitation and emission filters (Chroma Technology Corp.) with the excitation and emission
528 filters installed in Prior motorized filter wheels. A piezo electrically driven objective mount (PIFOC
529 model P-721, Physik Instrumente) was used to control movement in the z dimension. Step size for
530 z stacks was set at 0.2 μ m. Nikon Nis-Elements software was used to perform hardware control,
531 image capture and analysis. Images were deconvolved using a calculated point spread function
532 with the constrained iterative algorithm of Volocity (PerkinElmer). The quantitation module of
533 Volocity was used to calculate inter probe distances. To eliminate the possibility of measuring sister
534 chromatids, only alleles with single probe signals were analyzed.

536 Generation of knockout mice

537 Mouse work was approved by the UCSF IACUC, protocol number AN100466, and was conducted
538 in accordance with AALAC and NIH guidelines. The 12 kb acheiropodia associated sequence
539 (chr7:156,608,724-156,620,764; hg19) was converted to mouse sequence (chr5:29,335,354-
540 29,348,393; mm10) using the UCSC Genome Browser³⁶ liftOver tool. Two gRNA were designed to
541 target the 5' and 3' ends of this region (**Supplementary Table 3**) using the gRNA design tool on
542 the Integrated DNA Technologies (IDT) website and selected based on low off-target and high on-

543 target scores. The acheiropodia deletion allele was generated using *i-GONAD*³⁹. Briefly, after
544 reconstitution of two crRNA (IDT) and tracrRNA (IDT), these were mixed together (final
545 concentration 100 μ M each) and incubated at 92°C for 2 minutes and left at room temperature for
546 10 minutes to prepare the crRNA/tracrRNA complex. The genome-editing mixture, (30 μ M
547 crRNA/tracrRNA complex, 1 mg/ml Cas9 protein (IDT), Opti-MEM) was incubated at 37°C for 10
548 minutes. Estrus female FVB mice (Jackson Laboratory, catalog no. 001800) were mated to male
549 mice the night before. Presence of copulation plugs was confirmed by visual inspection the next
550 morning and the females having plugs were designated as Day 0.5 of gestation at noon and Day 0.7
551 of gestation at 16:00. Females on Day 0.7 were used for oviduct electroporation. Mice were
552 anesthetized using isoflurane, the ovary and oviducts were exposed by grasping the adipose tissue
553 surrounding the ovary. Approximately 1-2 μ l of the genome-editing mixture was injected into the
554 oviduct lumen upstream of the ampulla using a micropipette. Immediately following injection, the
555 oviduct was covered with a piece of wet paper soaked in PBS and then grasped by tweezer-type
556 electrodes (Bulldog Bio, catalog no. CUY652P2.5 X4). The electroporation was performed using a
557 square-wave pulse generator BTXECM830 (BTX Genetronics Inc.). The electroporation conditions
558 used were 8 pulses of 50 V at 5 mseconds wave length. After electroporation, the oviducts were
559 placed in their original position, and the muscle layer incision was sutured using absorbable suture
560 chromic gut. The coat layer incision was closed by AutoClip kit (Fine Science Tools, catalog no.
561 12022-09). The animals were kept on a warming pad (37°C) during surgery and monitored for
562 anesthesia recovery following surgery.

563

564 **Sanger sequencing and Southern blot**

565 PCR-Sanger sequencing (primers provided in **Supplementary Table 3**) was preformed using
566 standard techniques²⁸. For Southern blot analyses, genomic DNA were treated with *Bst*XI (New
567 England Biolabs, catalog no. R0113) and fractionated by agarose gel electrophoreses. Following
568 capillary transfer onto nylon membranes, blots were hybridized with Digoxigenin (DIG)-labeled
569 DNA probes (corresponding to chr5:29348565-29349037; mm10) amplified by the PCR DIG Probe
570 Synthesis Kit (Sigma-Aldrich, catalog no. 11636090910). The hybridized probe was
571 immunodetected with anti-digoxigenin Fab fragments conjugated to alkaline phosphatase (Sigma-
572 Aldrich, catalog no. 11093274910) and visualized with a CDP star (Sigma-Aldrich, catalog no.
573 11685627001) according to the manufacturer's protocol. Chemiluminescence was detected using
574 the FluorChem E (ProteinSimple, catalog no.92-14860-00).

575

576 **RT-qPCR**

577 Total RNA was collected from E11.5 limb buds or lymphoblastoid cells using TRIzol (Thermo
578 Fisher Scientific, catalog no. 15596026) and converted to cDNA using ReverTra Ace qPCR-RT
579 master mix with genomic DNA (gDNA) remover (Toyobo, catalog no. FSQ-301). qPCR was
580 performed using SsoFast EvaGreen supermix (Bio Rad, catalog no. 1725205). Primer sequences
581 used for qPCR are shown in **Supplementary Table 3**.

582

583 **Whole-mount *in situ* hybridization**

584 Mouse E11.5 embryos were fixed in 4% paraformaldehyde. A plasmid containing mouse *Shh*
585 cDNA (GenScript, catalog no. OMu22903D) was used as template for DIG-labeled probes. Mouse
586 whole-mount *in situ* hybridization was performed according to standard procedures⁶⁸.

587

588 **Bone and cartilage staining**

589 Embryos were harvested at E18.5 and limbs were dissected out and used for staining. Alcian
590 blue/Alizarin red staining was performed according to standard procedures for late-gestation stage
591 embryos⁶⁹.

592

593 **Analysis of CTCF Hi-ChIP data**

594 Analysis of the CTCF Hi-ChIP³⁵ data and figure generation were done using the HiCExplorer⁷⁰.

595

596 **Data Availability**

597 hg19 and hg38 human reference genome is available from NCBI [GenBank assembly](#)
598 ["GCA_000001405.1" \[https://www.ncbi.nlm.nih.gov/assembly/GCF_000001405.13/\]](#), and
599 ["GCA_000001405.15 \[https://www.ncbi.nlm.nih.gov/assembly/GCF_000001405.26/\]](#), respectively).
600 The deleted sequence information is available from Decipher database ["#411659](#)
601 [\[https://decipher.sanger.ac.uk/patient/411659/overview/general\]](#)". ChIP-seq and 4C-seq data are
602 available from the Gene Expression Omnibus under accession number ["GSE155324](#)
603 [\[https://www.ncbi.nlm.nih.gov/geo/query/acc.cgi?acc=GSE155324\]](#)". ENCODE data are available
604 from the ["UCSC genome browser \[https://genome.ucsc.edu/\]](#)". Hi-C datasets are available from the
605 ["3D Genome Browser \[http://www.3dgenome.org/\]](#)". The CTCF motif was obtained from ["JASPAR](#)
606 [\[http://jaspar.genereg.net/\]](#)". All other relevant data supporting the key findings of this study are

607 available within the article and its Supplementary Information files or from the corresponding author
608 upon reasonable request. A Source Data file accompanies the manuscript. A reporting summary
609 for this Article is available as a Supplementary Information file.

610

References

1. Freire-Maia, A., Freire-Maia, N., Morton, N. E., Azevêdo, E. S. & Quelce-Salgado, A. Genetics of acheiropodia (the handless and footless families of Brazil). VI. Formal genetic analysis. *Am. J. Hum. Genet.* **27**, 521–7 (1975).
2. Ianakiev, P. *et al.* Acheiropodia is caused by a genomic deletion in C7orf2, the human orthologue of the Lmbr1 gene. *Am. J. Hum. Genet.* **68**, 38–45 (2001).
3. Fagerberg, L. *et al.* Analysis of the human tissue-specific expression by genome-wide integration of transcriptomics and antibody-based proteomics. *Mol. Cell. Proteomics* **13**, 397–406 (2014).
4. Williamson, I. *et al.* Developmentally regulated Shh expression is robust to TAD perturbations. *Development* **146**, (2019).
5. Briscoe, J. & Théron, P. P. The mechanisms of Hedgehog signalling and its roles in development and disease. *Nat. Rev. Mol. Cell Biol.* **14**, 416–29 (2013).
6. Büscher, D., Bosse, B., Heymer, J. & Rütger, U. Evidence for genetic control of Sonic hedgehog by Gli3 in mouse limb development. *Mech. Dev.* **62**, 175–82 (1997).
7. Platt, K. A., Michaud, J. & Joyner, A. L. Expression of the mouse Gli and Ptc genes is adjacent to embryonic sources of hedgehog signals suggesting a conservation of pathways between flies and mice. *Mech. Dev.* **62**, 121–35 (1997).
8. Lewis, P. M. *et al.* Cholesterol modification of sonic hedgehog is required for long-range signaling activity and effective modulation of signaling by Ptc1. *Cell* **105**, 599–612 (2001).
9. Zeller, R., López-Ríos, J. & Zuniga, A. Vertebrate limb bud development: moving towards integrative analysis of organogenesis. *Nat. Rev. Genet.* **10**, 845–858 (2009).
10. Chiang, C. *et al.* Cyclopia and defective axial patterning in mice lacking Sonic hedgehog gene function. *Nature* **383**, 407–13 (1996).
11. Roessler, E. *et al.* Mutations in the human Sonic Hedgehog gene cause holoprosencephaly. *Nat. Genet.* **14**, 357–360 (1996).
12. VanderMeer, J. E. & Ahituv, N. cis-regulatory mutations are a genetic cause of human limb malformations. *Dev. Dyn.* **240**, 920–30 (2011).
13. Hill, R. E., Heaney, S. J. H. & Lettice, L. A. Sonic hedgehog: restricted expression and limb dysmorphologies. *J. Anat.* **202**, 13–20 (2003).
14. Petit, F., Sears, K. E. & Ahituv, N. Limb development: a paradigm of gene regulation. *Nat. Rev. Genet.* **18**, 245–258 (2017).

- 643 15. Shamseldin, H. E. *et al.* Novel copy number variants and major limb reduction malformation:
644 Report of three cases. *Am. J. Med. Genet. A* **170A**, 1245–1250 (2016).
- 645 16. Sagai, T., Hosoya, M., Mizushina, Y., Tamura, M. & Shiroishi, T. Elimination of a long-range
646 cis-regulatory module causes complete loss of limb-specific Shh expression and truncation of
647 the mouse limb. *Development* **132**, 797–803 (2005).
- 648 17. Phillips, J. E. & Corces, V. G. CTCF: master weaver of the genome. *Cell* **137**, 1194–211
649 (2009).
- 650 18. Schoenfelder, S. & Fraser, P. Long-range enhancer–promoter contacts in gene expression
651 control. *Nat. Rev. Genet.* **20**, 437–455 (2019).
- 652 19. Chang, L.-H., Ghosh, S. & Noordermeer, D. TADs and Their Borders: Free Movement or
653 Building a Wall? *J. Mol. Biol.* **432**, 643–652 (2020).
- 654 20. Fudenberg, G., Abdennur, N., Imakaev, M., Goloborodko, A. & Mirny, L. A. Emerging
655 Evidence of Chromosome Folding by Loop Extrusion. *Cold Spring Harb. Symp. Quant. Biol.*
656 **82**, 45–55 (2017).
- 657 21. Paliou, C. *et al.* Preformed chromatin topology assists transcriptional robustness of Shh
658 during limb development. *Proc. Natl. Acad. Sci. U. S. A.* **116**, 12390–12399 (2019).
- 659 22. Silveira, E. L. & Freire-Maia, A. Acheiropodia: new cases from Brazil. *Clin. Genet.* **54**, 256–7
660 (1998).
- 661 23. Firth, H. V *et al.* DECIPHER: Database of Chromosomal Imbalance and Phenotype in
662 Humans Using Ensembl Resources. *Am. J. Hum. Genet.* **84**, 524–33 (2009).
- 663 24. MacDonald, J. R., Ziman, R., Yuen, R. K. C., Feuk, L. & Scherer, S. W. The Database of
664 Genomic Variants: a curated collection of structural variation in the human genome. *Nucleic
665 Acids Res.* **42**, D986–92 (2014).
- 666 25. Karczewski, K. J. *et al.* The mutational constraint spectrum quantified from variation in
667 141,456 humans. *Nature* **581**, 434–443 (2020).
- 668 26. Landrum, M. J. *et al.* ClinVar: improving access to variant interpretations and supporting
669 evidence. *Nucleic Acids Res.* **46**, D1062–D1067 (2018).
- 670 27. Kothary, R. *et al.* A transgene containing lacZ inserted into the dystonia locus is expressed in
671 neural tube. *Nature* **335**, 435–7 (1988).
- 672 28. Laurell, T. *et al.* A novel 13 base pair insertion in the sonic hedgehog ZRS limb enhancer
673 (ZRS/LMBR1) causes preaxial polydactyly with triphalangeal thumb. *Hum. Mutat.* **33**, 1063–6
674 (2012).

- 675 29. VanderMeer, J. E. *et al.* A novel ZRS mutation leads to preaxial polydactyly type 2 in a
676 heterozygous form and Werner mesomelic syndrome in a homozygous form. *Hum. Mutat.* **35**,
677 945–8 (2014).
- 678 30. ENCODE Project Consortium. An integrated encyclopedia of DNA elements in the human
679 genome. *Nature* **489**, 57–74 (2012).
- 680 31. Guo, Y. *et al.* CRISPR Inversion of CTCF Sites Alters Genome Topology and
681 Enhancer/Promoter Function. *Cell* **162**, 900–10 (2015).
- 682 32. Merckenschlager, M. & Nora, E. P. CTCF and Cohesin in Genome Folding and Transcriptional
683 Gene Regulation. *Annu. Rev. Genomics Hum. Genet.* **17**, 17–43 (2016).
- 684 33. Grant, C. E., Bailey, T. L. & Noble, W. S. FIMO: scanning for occurrences of a given motif.
685 *Bioinformatics* **27**, 1017–8 (2011).
- 686 34. Krijger, P. H. L., Geeven, G., Bianchi, V., Hilvering, C. R. E. & de Laat, W. 4C-seq from
687 beginning to end: A detailed protocol for sample preparation and data analysis. *Methods* **170**,
688 17–32 (2020).
- 689 35. Mumbach, M. R. *et al.* HiChIRP reveals RNA-associated chromosome conformation. *Nat.*
690 *Methods* **16**, 489–492 (2019).
- 691 36. Kent, W. J. *et al.* The human genome browser at UCSC. *Genome Res.* **12**, 996–1006 (2002).
- 692 37. Yue, F. *et al.* A comparative encyclopedia of DNA elements in the mouse genome. *Nature*
693 **515**, 355–64 (2014).
- 694 38. Andrey, G. *et al.* Characterization of hundreds of regulatory landscapes in developing limbs
695 reveals two regimes of chromatin folding. *Genome Res.* **27**, 223–233 (2017).
- 696 39. Gurusurthy, C. B. *et al.* Creation of CRISPR-based germline-genome-engineered mice
697 without ex vivo handling of zygotes by i-GONAD. *Nat. Protoc.* **14**, 2452–2482 (2019).
- 698 40. Diehl, A. G., Ouyang, N. & Boyle, A. P. Transposable elements contribute to cell and
699 species-specific chromatin looping and gene regulation in mammalian genomes. *Nat.*
700 *Commun.* **11**, 1796 (2020).
- 701 41. Lupiáñez, D. G. *et al.* Disruptions of Topological Chromatin Domains Cause Pathogenic
702 Rewiring of Gene-Enhancer Interactions. *Cell* **161**, 1012–1025 (2015).
- 703 42. Wang, Y. *et al.* The 3D Genome Browser: a web-based browser for visualizing 3D genome
704 organization and long-range chromatin interactions. *Genome Biol.* **19**, 151 (2018).
- 705 43. Dixon, J. R. *et al.* Topological domains in mammalian genomes identified by analysis of
706 chromatin interactions. *Nature* **485**, 376–80 (2012).

- 707 44. Symmons, O. *et al.* The Shh Topological Domain Facilitates the Action of Remote Enhancers
708 by Reducing the Effects of Genomic Distances. *Dev. Cell* **39**, 529–543 (2016).
- 709 45. Downen, J. M. *et al.* Control of Cell Identity Genes Occurs in Insulated Neighborhoods in
710 Mammalian Chromosomes. *Cell* **159**, 374–387 (2014).
- 711 46. Arzate-Mejía, R. G., Recillas-Targa, F. & Corces, V. G. Developing in 3D: the role of CTCF in
712 cell differentiation. *Development* **145**, dev137729 (2018).
- 713 47. Sparago, A. *et al.* Microdeletions in the human H19 DMR result in loss of IGF2 imprinting and
714 Beckwith-Wiedemann syndrome. *Nat. Genet.* **36**, 958–960 (2004).
- 715 48. Katainen, R. *et al.* CTCF/cohesin-binding sites are frequently mutated in cancer. *Nat. Genet.*
716 **47**, 818–821 (2015).
- 717 49. Norton, H. K. & Phillips-Cremins, J. E. Crossed wires: 3D genome misfolding in human
718 disease. *J. Cell Biol.* **216**, 3441–3452 (2017).
- 719 50. Zhang, J. *et al.* International Cancer Genome Consortium Data Portal--a one-stop shop for
720 cancer genomics data. *Database (Oxford)*. **2011**, bar026 (2011).
- 721 51. Ji, X. *et al.* 3D Chromosome Regulatory Landscape of Human Pluripotent Cells. *Cell Stem*
722 *Cell* **18**, 262–275 (2016).
- 723 52. Li, H. & Durbin, R. Fast and accurate short read alignment with Burrows-Wheeler transform.
724 *Bioinformatics* **25**, 1754–60 (2009).
- 725 53. McKenna, A. *et al.* The Genome Analysis Toolkit: a MapReduce framework for analyzing
726 next-generation DNA sequencing data. *Genome Res.* **20**, 1297–303 (2010).
- 727 54. Purcell, S. *et al.* PLINK: a tool set for whole-genome association and population-based
728 linkage analyses. *Am. J. Hum. Genet.* **81**, 559–75 (2007).
- 729 55. Layer, R. M., Chiang, C., Quinlan, A. R. & Hall, I. M. LUMPY: a probabilistic framework for
730 structural variant discovery. *Genome Biol.* **15**, R84 (2014).
- 731 56. Robinson, J. T. *et al.* Integrative genomics viewer. *Nat. Biotechnol.* **29**, 24–6 (2011).
- 732 57. Pu, X., Young, A. P. & Kubisch, H. M. Production of Transgenic Mice by Pronuclear
733 Microinjection. in 17–41 (2019). doi:10.1007/978-1-4939-8831-0_2
- 734 58. Pennacchio, L. A. *et al.* In vivo enhancer analysis of human conserved non-coding
735 sequences. *Nature* **444**, 499–502 (2006).
- 736 59. Landt, S. G. *et al.* ChIP-seq guidelines and practices of the ENCODE and modENCODE
737 consortia. *Genome Res.* **22**, 1813–31 (2012).
- 738 60. Zhang, Y. *et al.* Model-based analysis of ChIP-Seq (MACS). *Genome Biol.* **9**, R137 (2008).

- 739 61. Amemiya, H. M., Kundaje, A. & Boyle, A. P. The ENCODE Blacklist: Identification of
740 Problematic Regions of the Genome. *Sci. Rep.* **9**, 9354 (2019).
- 741 62. Ross-Innes, C. S. *et al.* Differential oestrogen receptor binding is associated with clinical
742 outcome in breast cancer. *Nature* **481**, 389–393 (2012).
- 743 63. Fornes, O. *et al.* JASPAR 2020: update of the open-access database of transcription factor
744 binding profiles. *Nucleic Acids Res.* **48**, D87–D92 (2020).
- 745 64. Quinlan, A. R. & Hall, I. M. BEDTools: a flexible suite of utilities for comparing genomic
746 features. *Bioinformatics* **26**, 841–2 (2010).
- 747 65. van de Werken, H. J. G. *et al.* Robust 4C-seq data analysis to screen for regulatory DNA
748 interactions. *Nat. Methods* **9**, 969–72 (2012).
- 749 66. Eskeland, R. *et al.* Ring1B Compacts Chromatin Structure and Represses Gene Expression
750 Independent of Histone Ubiquitination. *Mol. Cell* **38**, 452–464 (2010).
- 751 67. Morey, C., Da Silva, N. R., Perry, P. & Bickmore, W. A. Nuclear reorganisation and chromatin
752 decondensation are conserved, but distinct, mechanisms linked to Hox gene activation.
753 *Development* **134**, 909–919 (2007).
- 754 68. Hargrave, M., Bowles, J. & Koopman, P. In situ hybridization of whole-mount embryos.
755 *Methods Mol. Biol.* **326**, 103–13 (2006).
- 756 69. Rigueur, D. & Lyons, K. M. Whole-mount skeletal staining. *Methods Mol. Biol.* **1130**, 113–121
757 (2014).
- 758 70. Wolff, J. *et al.* Galaxy HiCExplorer 3: a web server for reproducible Hi-C, capture Hi-C and
759 single-cell Hi-C data analysis, quality control and visualization. *Nucleic Acids Res.* **48**, W177–
760 W184 (2020).
- 761 71. Yates, A. D. *et al.* Ensembl 2020. *Nucleic Acids Res.* **48**, D682–D688 (2020).

762
763
764 **# University of Washington Center for Mendelian Genomics**

765 [Michael J. Bamshad^{6,7,8} & Deborah A. Nickerson^{7,8}](#)

766 [Non-contributing members of the consortium are listed within the Supplementary Information file.](#)

767
768
769
770

771
772
773
774
775
776
777
778
779
780
781
782
783
784
785
786
787
788
789
790
791
792
793
794
795
796
797
798
799
800
801
802

Acknowledgments

We would first and foremost like to thank the family for participating in this study. We would also like to acknowledge Julia E. VanderMeer for initiating this study, Maya Vella and Marcelo R Luizon for their assistance with this project, Jorge Oksenberg and Stacy Caillier for help with lymphoblastoid cell line generation, Iain Williamson for his FISH expertise and Martin Kircher, Malte Spielman and Loïc Defontaine for assistance with whole-genome sequencing data analyses. This work was supported in part by grant numbers 1R01HD059862 and 1P01HD084387 from the National Institute of Child Health and Human Development (NICHD) and grant number 1R019576103 from the National Human Genome Research Institute (NHGRI) (N.A.). A.U. was supported by the Japan Society for the Promotion of Science (JSPS) postdoctoral fellowships for research abroad and the Uehara Memorial Foundation postdoctoral fellowship. L.K was funded by PhD studentship from the UK Medical Research Council (MRC) and LAL by an MRC University Unit grant MM_UU_00007/8. Sequencing was provided by the University of Washington - Center for Mendelian Genomics (UW-CMG) and was funded by NHGRI and NHLBI grants UM1 HG006493 and U24 HG008956 and by the Office of the Director, NIH under Award Number S10OD021553. The content is solely the responsibility of the authors and does not necessarily represent the official views of the National Institutes of Health. F.P. received a research grant from the Fulbright program.

Author contributions

A.U., F.P. and N.A. conceived and designed the study. C.X. helped in lymphoblastoid generation. A.U. performed ChIP-seq, 4C-seq and generated knockout mice. L.K. and L.A.L. performed and analyzed DNA FISH. A.U. and Y.Z. analyzed the phenotype of knockout mice. Y.Z. constructed the LacZ plasmid. M.J.B., D.A.N. and the University of Washington Center for Mendelian Genomics carried out the whole-genome sequencing. F.P. analyzed whole-genome sequencing data. F.P. and C.X. carried out and analyzed Sanger sequencing. J.Z., I.G-S., K.J., and Y.S. performed computational analyses. A.U., F.P., and N.A. interpreted the data. A.U., F.P. and N.A. wrote the manuscript.

Competing Interests

803 There are no competing interests.

804

805 **Figure Legends**

806

807 **Fig. 1 | Fine-mapping of the acheiropodia-associated deletion.** **a**, Pedigree of acheiropodia
808 family with proband indicated via the arrow. Squares and circles represent males and females,
809 respectively. **b**, WGS alignments showing a homozygous 12 kb deletion in the acheiropodia
810 proband. The Y-axis is the read depth (number of reads for each nucleotide). The deletion appears
811 in a heterozygous manner in both parents. BP: breakpoint; P: proband; M: mother; F: father. **c**,
812 PCR amplification using three different primers pairs, whose location is indicated in **b**, further
813 confirming the breakpoint in the proband (P) and mother (M) and father (F). **PCR was performed**
814 **several times using different primer sets to validate the deletion.** **d**, Sanger sequencing of the
815 acheiropodia patient showing the breakpoint sequence which also has a CA insertion.

816

817 **Fig. 2 | Mouse transgenic enhancer assay for the 12 kb acheiropodia-associated sequence.**
818 Schematic representation of the mouse transgenic enhancer assay (upper panel) showing the 12
819 kb acheiropodia associated sequence cloned upstream of *Hsp68* promoter-LacZ gene. Enhancer
820 activity, as visualized by LacZ staining, was not observed in the ZPA for the six PCR positive E11.5
821 mouse embryos (lower panel).

822

823 **Fig. 3 | CTCF and RAD21 distribution in the *LMBR1-SHH* locus.** **a**, CTCF and RAD21 ChIP-seq
824 enrichment in lymphoblastoid cells from wildtype (WT) and proband (Mut) at the *LMBR1-SHH* locus.
825 GM12878 (lymphoblastoid cell line) TAD boundaries are shown in orange and gray horizontal bar.
826 ZRS and the acheiropodia-associated deleted region are shown in orange and blue vertical lines
827 respectively. CTCF orientations are shown as red triangles. The Y-axis is the signal p-value to
828 reject the null hypothesis that the signal at that location is present in the control. **b**, Zoom in of the
829 region around the *LMBR1* gene. **c**, CTCF motif from JASPAR⁶³ [<http://jaspar.genereg.net/>] and
830 CTCF motif scores, as assigned by FIMO³³, overlapping CTCF peaks in the *LMBR1* locus.

831

832 **Fig. 4 | Chromatin interactions with the *SHH* promoter.** **a**, 4C contact profiles in lymphoblastoid
833 cells from wildtype (WT) and proband (Mut) at the *LMBR1-SHH* locus. The viewpoint is depicted by
834 a black arrowhead. The median and 20th and 80th percentiles of sliding 2-50 kb windows
835 determine the main trend line. The color scale represents enrichment relative to the maximum
836 medium value attainable at 12 kb resolution. CTCF and RAD21 ChIP-seq peaks are shown as

837 black and blue vertical line respectively. The ZRS and the acheiropodia-associated deleted region
838 are shown as orange and blue vertical lines respectively. CTCF orientations are shown as red
839 triangles. **b**, Zoom in of the region around the *LMBR1* gene.

840

841 **Figure 5 | DNA FISH showing the *SHH* promoter interaction with the acheiropodia-**
842 **associated region. a**, Schematic of the *LMBR1-SHH* locus showing the ZRS and the
843 acheiropodia-associated deleted region via orange and blue vertical lines respectively. CTCF
844 orientations are shown as red triangles and the locations to which the DNA FISH probes hybridize
845 to are depicted by blue bars. **b**, Images of representative nuclei from DNA FISH analysis of
846 parental and proband lymphoblastoid cells showing FISH signals for SHH, LSC2, LSC3-5 and 12kb
847 probes. Scale bars: 5 μ m. **c**, Violin plots showing the distribution of interprobe distances (μ m)
848 between SHH – LSC1, SHH – LSC2 and SHH – Deletion. The wild type allele was distinguished
849 from the mutant allele in the parental cell line using the 12kb probe. SHH – deletion is measured
850 from SHH to 12kb probe on the wild type allele and from SHH to LSC3-5 probe on the mutant allele.
851 The statistical significance between data sets was examined by a two-sided Mann–Whitney U-test,
852 ** = 0.004537 and **** = 2.083×10^{-11} (n= 75-150 alleles).

853

854 **Fig. 6 | Human and mouse genomic comparisons and phenotype of mice where the**
855 **orthologous region was deleted. a**, Comparison of the *LMBR1-SHH* locus between human and
856 mice. CTCF site deletions analyzed by Paliou *et al.*²¹ are marked by purple lines and those
857 generated by #, Williamson *et al.*⁴ are denoted by yellow lines or gray rectangle, and marked by *.
858 CTCF motif orientation is shown via red triangles. The acheiropodia-associated deletion and its
859 mouse orthologous sequence are depicted by a blue rectangle. Mouse limb CTCF ChIP-seq data
860 from ENCODE³⁷, Andrey *et al.*³⁸, Paliou *et al.*²¹ and human CTCF ChIP-seq data from this study
861 (WT= wild type; Mut= proband) are shown as black genomic tracks below the locus. The
862 conservation track is adopted from the Ensembl Genome Browser⁷¹ with green lines indicating
863 conserved sequences between humans and mice. **b**, *Shh* gene expression levels dissected from
864 E11.5 mouse autopods from wild type (WT) and knockout (KO) mice as determined by qRT-PCR.
865 Each value represents the ratio of *Shh* gene expression to that of β -*Actin*, and values are mean \pm
866 standard deviation. The expression value of WT group was arbitrarily set at 1.0. Each dot
867 represents one embryo and statistical differences were determined using a **two-sided unpaired t**
868 **test** ($P= 0.7796$, N.S., not significant). Source data are provided as a Source Data file. **c**, Whole-

869 mount *in situ* hybridization for *Shh* of wild type (WT) and knockout (KO) E11.5 mouse embryos.
870 Forelimbs (FL) and hindlimbs (HL) were dissected and shown in the lower panel. **d**, Wild type (WT)
871 and knockout (KO) E18.5 limb skeletal staining using alizarin red/alcian blue.

872

873 **Fig. 7 | Proposed model for the aberrant chromatin structure of the *LMBR1-SHH* locus in the**
874 **acheiropodia patient.** Model of chromatin structure in the *LMBR1-SHH* locus based on our CHIP-
875 seq and 4C-seq data. CTCF sites are shown as red triangles and the cohesin complex is shown as
876 a green ring. The ZRS is depicted as an orange oval.

877

878

Figure 1

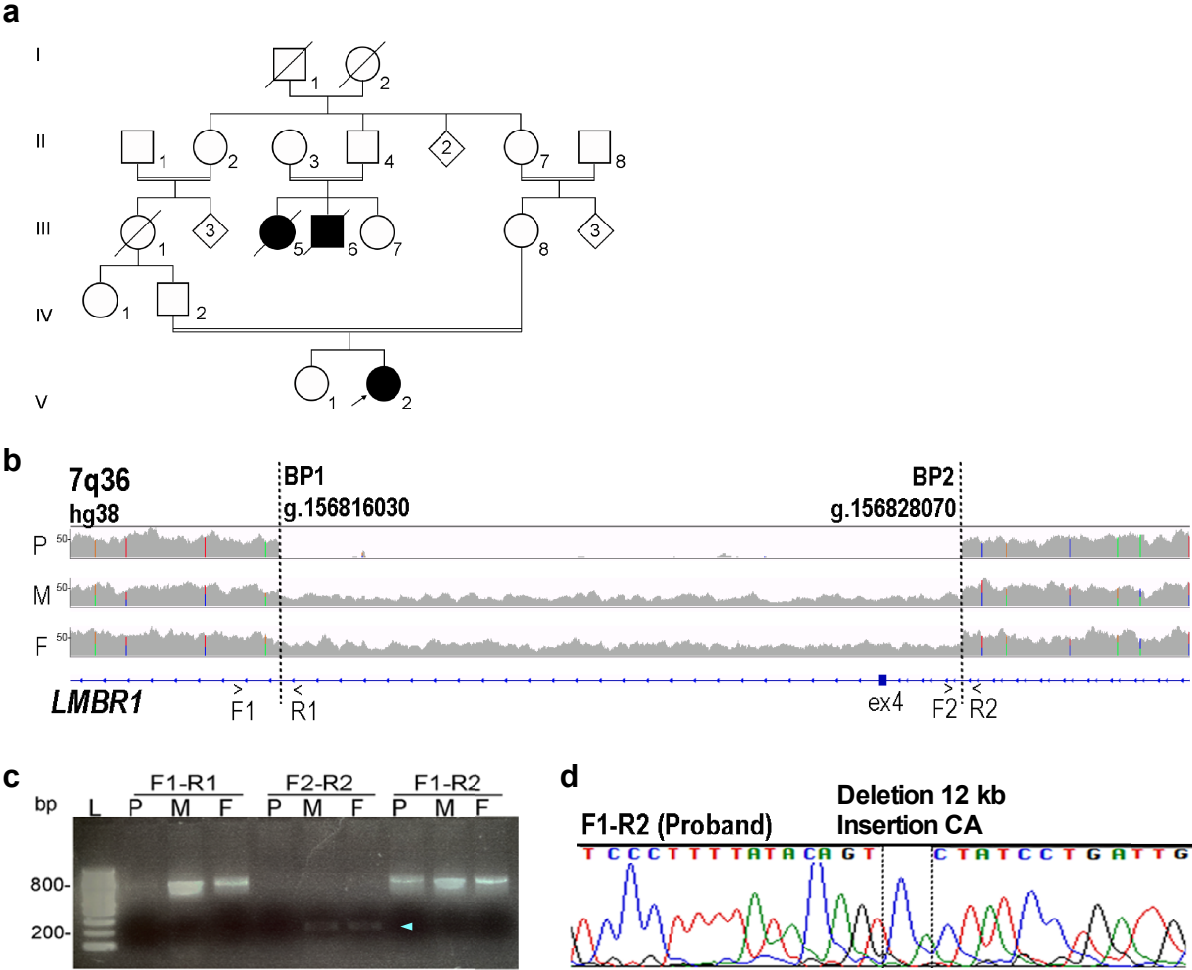


Figure 2

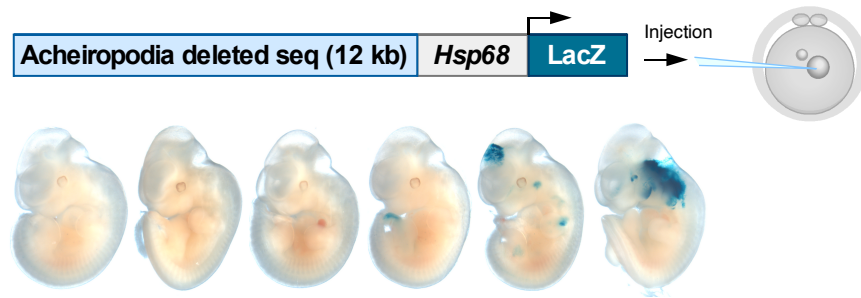


Figure 3

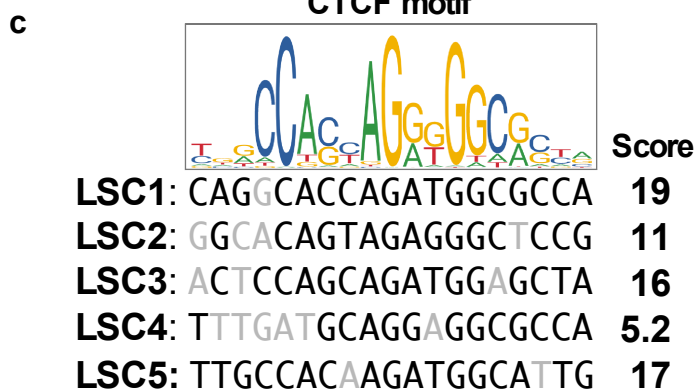
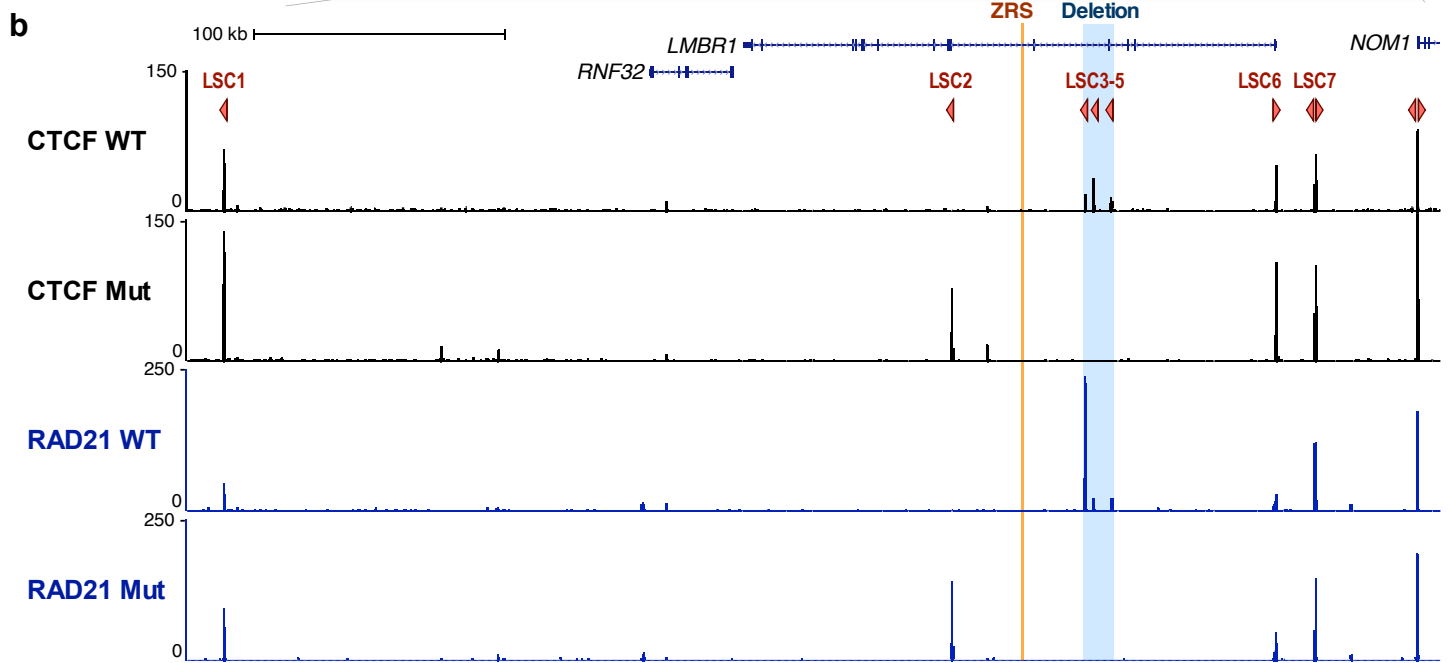
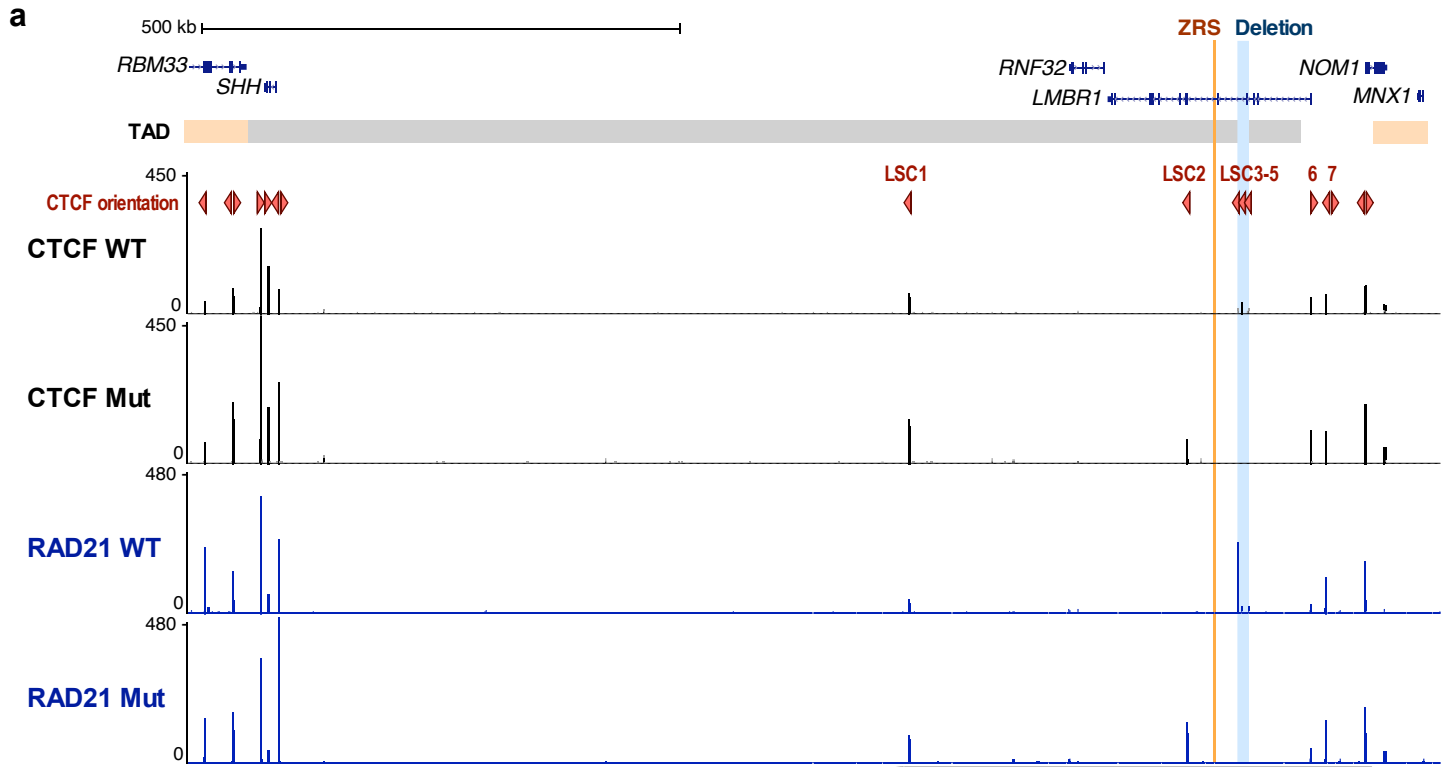


Figure 4

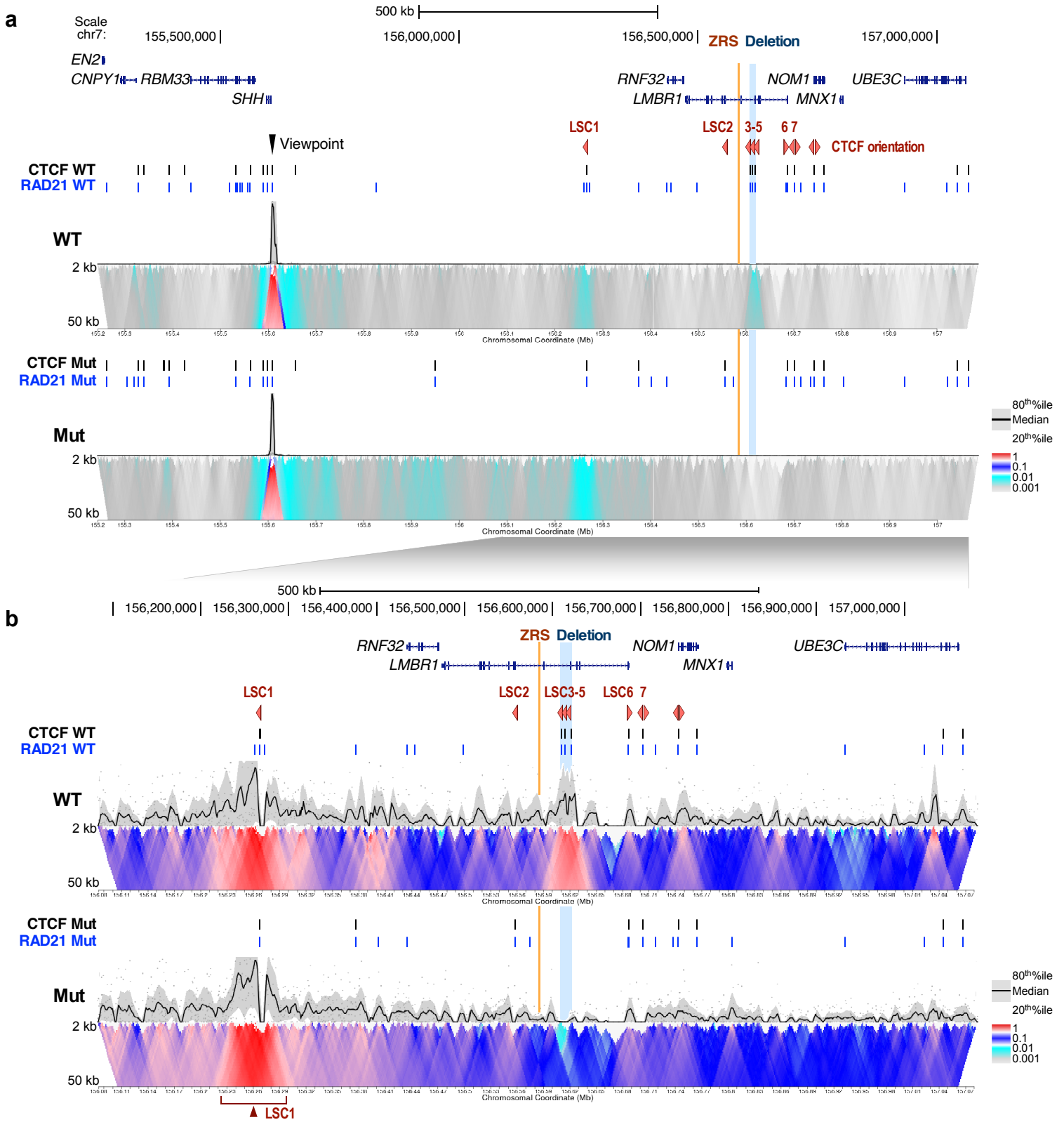


Figure 5

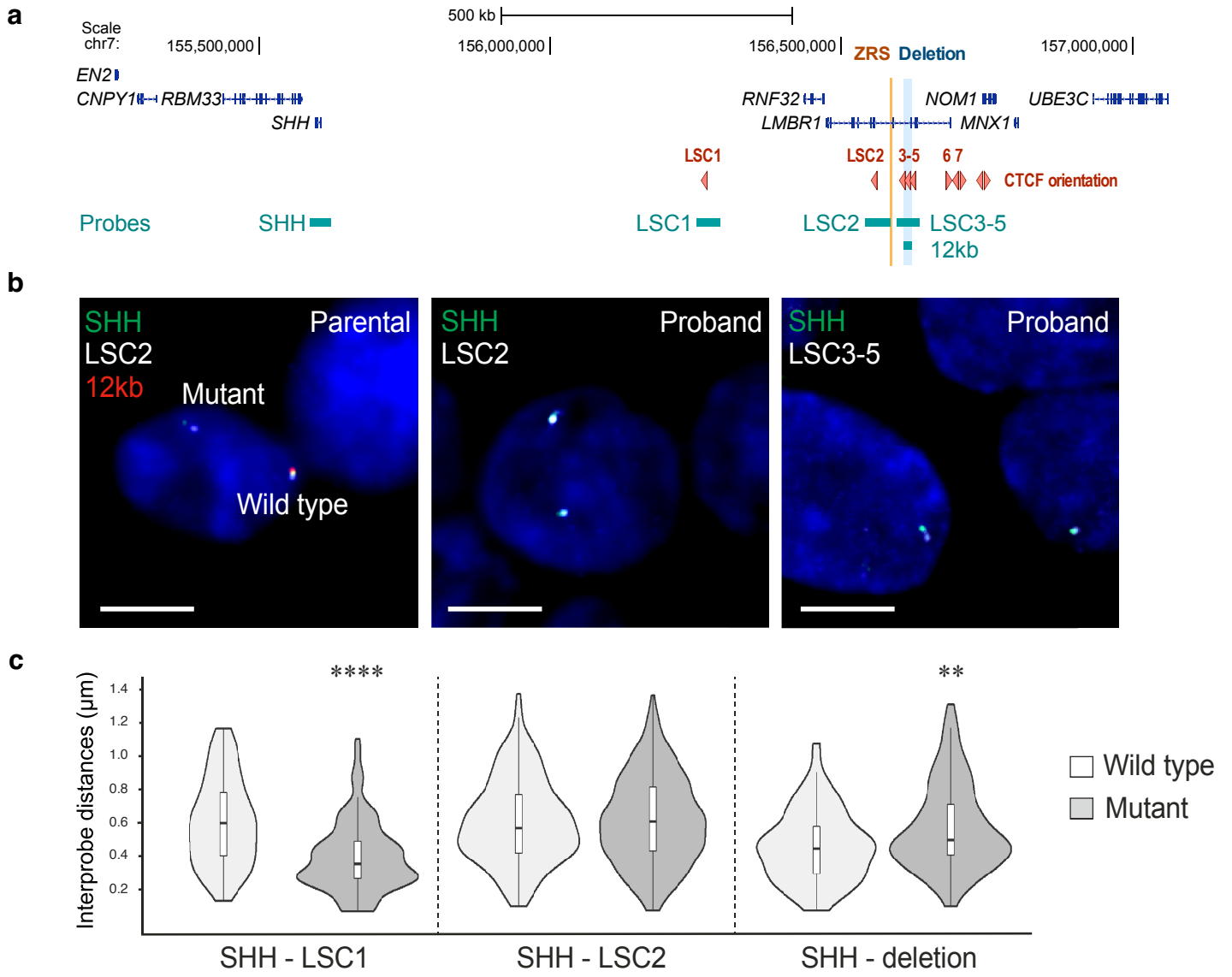


Figure 6

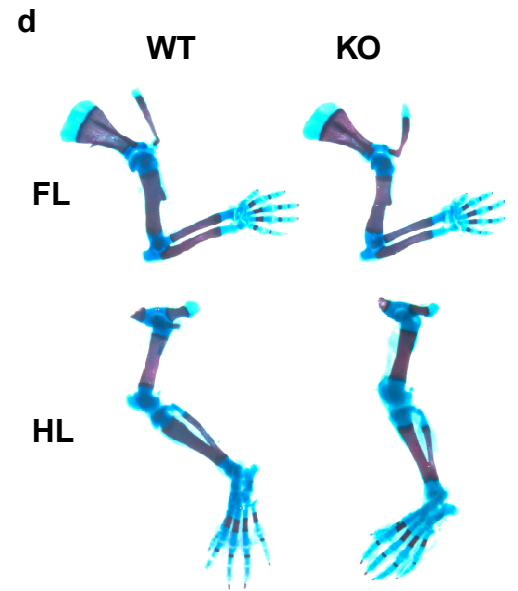
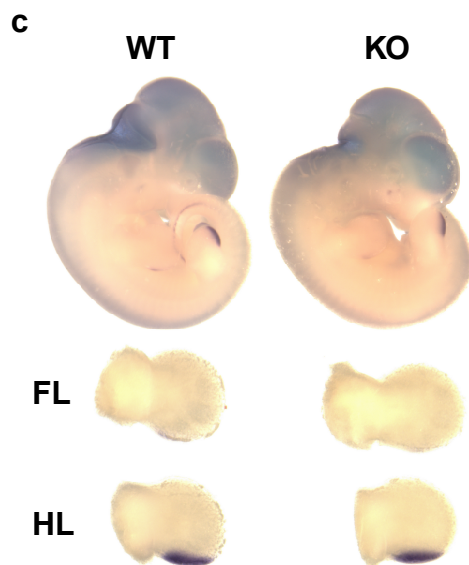
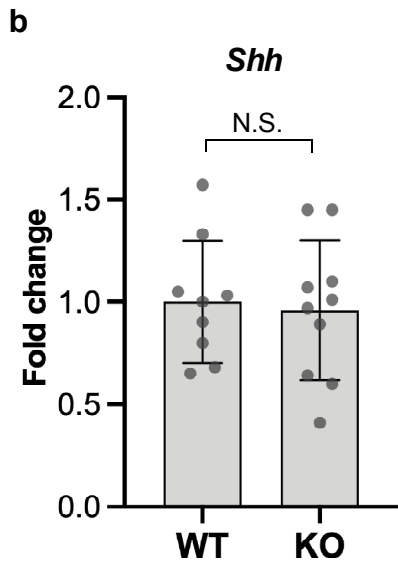
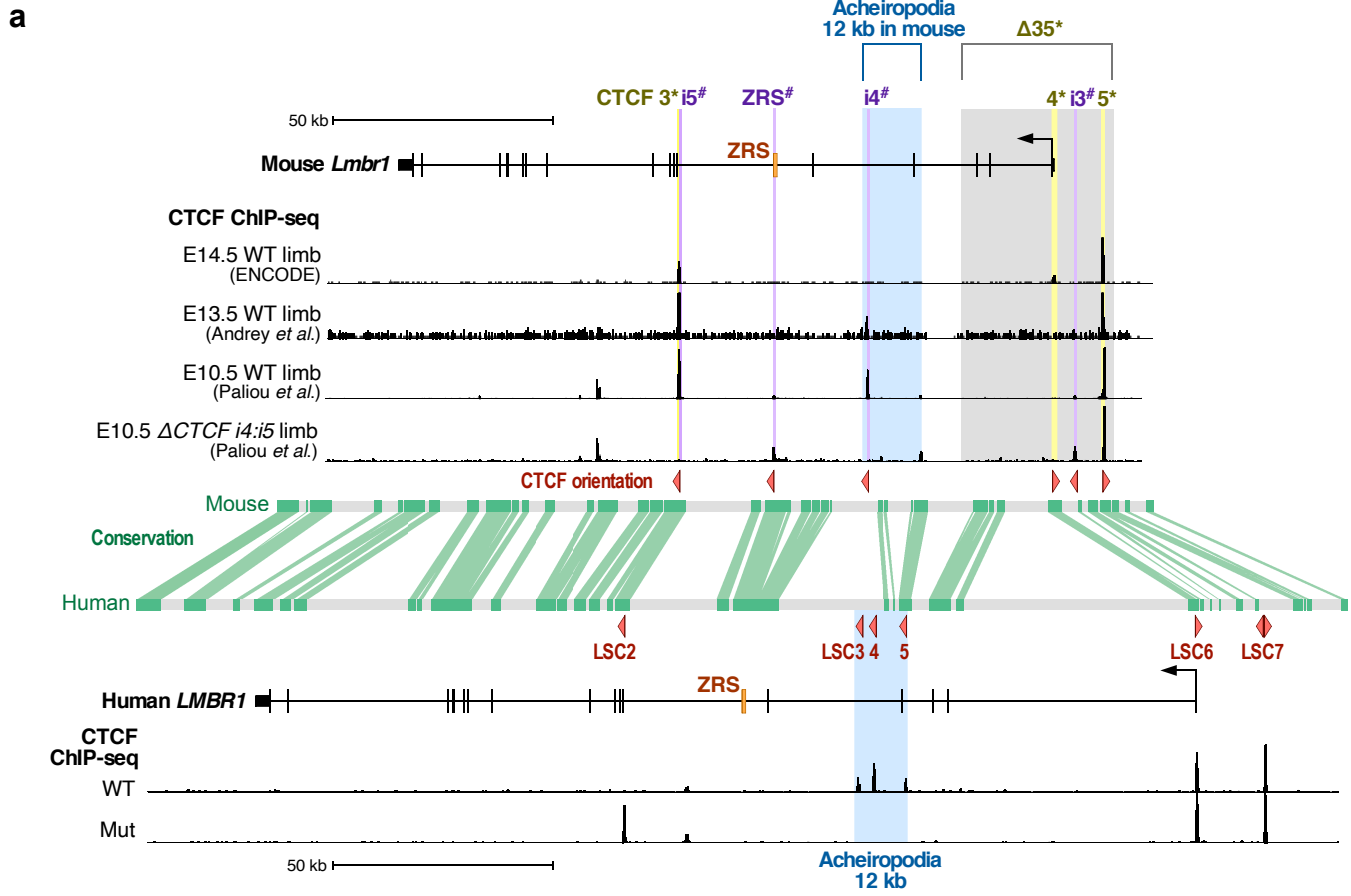


Figure 7

